J. Fluid Mech. (2004), *vol.* 512, *pp.* 1–19.
DOI: 10.1017/S0022112004008766 Printed in the United Kingdom

Estimation of viscosity profiles using velocimetry data from parallel flows of linearly viscous fluids: application to microvascular haemodynamics

By E. R. DAMIANO[1], D. S. LONG[1] AND M. L. SMITH[2]

[1]Department of Mechanical and Industrial Engineering, University of Illinois at Urbana-Champaign, Urbana, IL 61801, USA

[2]Department of Biomedical Engineering, University of Virginia Health Science Center, Charlottesville, VA 22908, USA

(Received 22 August 2003 and in revised form 24 November 2003)

An approach is presented that uses velocimetry data to estimate accurately the spatial distribution of viscosity in steady laminar parallel flows of incompressible linearly viscous fluids. The approach is generally applicable to Newtonian fluids with spatially varying viscosity or to particle-suspension flows where a non-uniform distribution of the particles contributes to spatial variations in the local effective viscosity of the suspension. Emphasis is placed on the application of these methods to steady axisymmetric blood flow in cylindrical glass capillary tubes and microvessels. In this context, the spatial variations in viscosity over the vessel cross-section are predicted where it is assumed that the rheological properties associated with a heterogeneous red blood cell suspension can be well approximated by a continuous generalized linearly viscous fluid having a spatially non-uniform viscosity. For such a fluid, an expression for the viscosity profile over the vessel cross-section is derived that satisfies the conservation principles of mass and momentum and depends upon the *a priori* determined velocity distribution, which is extracted from fluorescent micro-particle image velocimetry data obtained from microvessels *in vivo*. These profiles provide useful information about dynamic, kinematic and rheological properties of the flow that include expressions for the axial pressure-gradient component, the local shear stress distribution, and the relative apparent viscosity. In microvessels, the effect of the glycocalyx surface layer on the vessel wall is also accounted for in the analysis by modelling the layer as a uniformly thick porous medium. Velocimetry data are presented from *in vivo* measurements made in venules after the application of a light-dye treatment to degrade the glycocalyx. Results reveal that these methods are sufficiently sensitive to detect a reduction in glycocalyx thickness of $\sim 0.3\,\mu m$, which represents a fractional decrease in thickness of ~ 60–70% when compared with results from a separately published data set obtained from venules having an intact glycocalyx.

1. Introduction

It is well known that blood, consisting primarily of red cells and plasma, undergoes a phase separation in these two constituents under steady flow in microvessels and narrow glass capillary tubes (Cokelet 1999; Pries, Neuhaus & Gaehtgens 1992). This non-uniform distribution of red cells over the vessel cross-section leads to a cell-rich core flow and a plasma-rich region near the wall. Fluid drag in the plasma-rich

region gives rise to the so-called Fåhræus effect, in which the instantaneous volume fraction of red cells in the vessel, or tube haematocrit, H_T, is decreased relative to the red-cell concentration discharged from the vessel, or discharge haematocrit, H_D. The ratio H_T/H_D is seen to decrease with decreasing vessel diameter in glass tubes ranging between ~ 20 and 1000 μm in diameter (Cokelet 1999). Furthermore, since disproportionate amounts of the shear-rate and velocity variations over the vessel cross-section are associated with flow in the less viscous plasma-rich region, the relative apparent viscosity, η_{rel}, defined as the ratio of steady volume-flow rates per unit pressure drop of blood plasma relative to whole blood, is also seen to decrease with decreasing vessel diameter in glass tubes ranging between ~ 10 and 1000 μm in diameter. This phenomenon, known as the Fåhræus–Lindqvist effect, has been fairly well established *in vitro* for blood flow under high shear rates through smooth-walled glass capillary tubes (Pries *et al.* 1992).

For steady flow in glass capillary tubes, vessel diameter and discharge haematocrit are the most important determinants of a variety of flow parameters, including H_T, η_{rel}, the volume-flow rate, Q, the axial pressure-gradient component, $\mathrm{d}p/\mathrm{d}z$, and the local shear stress, τ_{rz}. Owing to the significant heterogeneity in red-cell distributions that arises within microvascular networks *in vivo*, H_D can typically assume a broad range of values for the many vessels in a given network, and even a significant variability in its value for a particular vessel in the network over time. This heterogeneity, coupled with the inability to measure pressure gradients accurately *in vivo* (Lipowsky, Kovalcheck & Zweifach 1978; Lipowsky, Usami & Chien 1980), has confounded attempts at quantitatively characterizing blood flow in the microcirculation.

Here we present a method for easily estimating all of the aforementioned rheological parameters, in both glass capillary tubes and individual microvessels within a microvascular network, based on an analytical expression for the viscosity profile derived from the cross-sectional velocity distribution obtained using fluorescent micro-particle image velocimetry (μ-PIV). Estimation of H_T and H_D further requires knowledge of the dependence of blood viscosity on haematocrit as might be obtained from rotational viscometric studies of red blood cell suspensions in blood plasma. Although our emphasis is on microhaemofluidics, and the approach will be illustrated in the context of that example, these methods are generally applicable to any steady laminar parallel flow of an incompressible Newtonian fluid or particle suspension that has a non-uniform viscosity variation over the flow cross-section.

One further consideration regarding microhaemofluidics in microvessels pertains to a macromolecular carbohydrate-rich surface layer on the vascular endothelium known as the glycocalyx. Recent studies in capillaries and venules estimate the glycocalyx to be ~ 0.3–0.5 μm thick *in vivo* (Vink & Duling 1996; Smith *et al.* 2003; Long *et al.* 2004). Microfluidic studies near the vessel wall using high-resolution fluorescent μ-PIV in post-capillary venules *in vivo* revealed nearly complete retardation of plasma flow through the glycocalyx (Smith *et al.* 2003). Although such a structure accounts for only ~ 2–3% of the radius of vessels 30–50 μm in diameter, it happens to reside in the high-shear-rate low-viscosity plasma-rich region near the vessel wall. As such, even a relatively thin glycocalyx with sufficiently low permeability could effectively immobilize a substantial fraction of plasma and therefore be an important determinant of η_{rel} and $\mathrm{d}p/\mathrm{d}z$ (Damiano 1998). In particular, for a Poiseuille flow of a constant-viscosity fluid, the removal of a 0.5-μm-thick glycocalyx would lead only to an 8 to 14% decrease in apparent viscosity in vessels ranging from 50 down to 30 μm in diameter. On the other hand, Damiano (1998) showed that, under the same conditions, a 30 to 40% decrease in apparent viscosity could be expected if the fluid were

non-uniformly viscous in a way that approximates the viscosity distribution of a particulate suspension like blood. Therefore, by virtue of the non-uniform distribution of red cells in microvessels, the glycocalyx can exert a significant influence on microvascular resistance in vessels as large as 50 μm in diameter. Following methods of Damiano *et al.* (1996), we will be treating the glycocalyx surface layer as a porous medium with a vanishingly small solid-volume fraction.

2. Microhaemofluidics in cylindrical tubes

The model that forms the basis of our viscosity-profile estimate depends upon the assumption that in tubes and vessels larger than 20 μm in diameter, the rheological properties associated with a particulate red blood cell suspension can be well approximated by a continuous linearly viscous fluid having a spatially non-uniform viscosity. Cokelet (1999) found support for the continuum approximation in his studies using physiological concentrations of red blood cells suspended in plasma flowing at physiological shear rates in glass tubes as small as 20 μm in diameter. Results of the analysis presented here, when applied to μ-PIV data obtained in glass capillary tubes and microvessels greater than 20 μm in diameter (Long *et al.* 2004), add further support to the validity of this approximation.

Under physiologically typical flow rates in microvessels, results have consistently shown (Long *et al.* 2004) that over $\sim 90\%$ of the vessel cross-section, shear rates exceed $\sim 50\,\mathrm{s}^{-1}$. Rotational viscometric data of mouse and human red blood cell suspensions in Ringer's solution (Chen & Kaul 1994) or autologous blood plasma (Long, Smith, Ley & Damiano, unpublished data) have shown that, at shear rates in excess of $\sim 50\,\mathrm{s}^{-1}$, blood viscosity at fixed physiologically typical haematocrits varies by less than 50% over an order of magnitude change in shear rate. Thus, in such flow regimes, it might be reasonable to regard a heterogeneous suspension such as blood as being a generalized linearly viscous fluid in the sense that the Cauchy stress tensor, $\boldsymbol{\sigma}$, is a linear function of the rate of deformation tensor, $\boldsymbol{D}$, while the viscosity, μ, is independent of $\boldsymbol{D}$ but may depend on thermodynamic state (as defined, for example, by the density, ρ, and temperature, T) and local haematocrit, H, namely $\mu = \mu(\rho, T, H)$. More generally, if a linear relationship exists between $\boldsymbol{\sigma}$ and $\boldsymbol{D}$, we can regard both homogeneous and heterogeneous fluids as linearly viscous so long as spatial variations in viscosity can come about as a result of variations in variables such as temperature or particulate concentration (e.g. haematocrit), but not as a result of variations in shear rate. In this sense, the dependence of blood viscosity on haematocrit (as with temperature in a classical Newtonian fluid, for example) enters into the analysis as a transport relation, which is empirically derived from species-specific rotational viscometric data. In what follows, we shall limit our attention to generalized linearly viscous fluids defined in the manner in which they have been described here.

Whereas most two-phase and variable-viscosity models of blood flow in the microcirculation that invoke the continuum approximation have started with assumptions about the viscosity and/or haematocrit distributions that led to predictions of the velocity profile (Thomas 1962; Nair, Hellums & Olson 1989; Secomb 1995; Damiano 1998; Sharan & Popel 2001), we shall proceed by solving the inverse problem. Taking the velocity distribution to be known from fluorescent μ-PIV data, we shall derive a simple analytical expression for the viscosity profile over the vessel cross-section that satisfies the conservation principles of mass and momentum and depends only upon the experimentally obtained velocity distribution. Once obtained, these profiles provide useful information about dynamic, kinematic and rheological properties of the flow.

2.1. *The momentum equation*

For a fully developed axisymmetric steady flow of a purely viscous isotropic incompressible fluid in a rigid smooth-walled circular cylinder of radius R, the continuity and axial momentum equations in cylindrical coordinates (r, θ, z) are both integrable in r, provided that the pressure does not vary over the tube cross-section and that the viscous normal stress component, τ_{zz}, is either independent of z or identically zero (as would typically arise in fully developed flow). Without any further specificity on the deviatoric stress tensor, $\boldsymbol{\tau}$, we obtain the general result for this flow regime relating the viscous shear stress component, τ_{rz}, and the pressure, p, given by

$$\frac{1}{r}\frac{\partial}{\partial r}(r\tau_{rz}) = \frac{\mathrm{d}p}{\mathrm{d}z} = \text{constant} \quad \Longrightarrow \quad \tau_{rz} = \frac{r}{2}\frac{\mathrm{d}p}{\mathrm{d}z} \quad (0 < r < R). \tag{2.1}$$

Therefore, independent of the constitutive behaviour of the fluid, τ_{rz} grows linearly in absolute value from zero at the tube centre to a maximum at the tube wall. Thus in this flow regime, the shear stress distribution for any purely viscous incompressible fluid is of the same form as would arise in a Poiseuille flow in the tube.

2.2. *The viscosity distribution for a linearly viscous fluid*

For a linearly viscous fluid with radially varying viscosity, $\mu(r)$, the constitutive relationship between the local shear rate, $\dot{\gamma}(r)$, and τ_{rz} is given for this flow regime by $\tau_{rz} = \mu(r)\dot{\gamma}(r)$, which, when combined with the result from the conservation of momentum given in (2.1), provides

$$\tau_{rz} = \mu(r)\frac{\mathrm{d}v_z}{\mathrm{d}r} = \frac{r}{2}\frac{\mathrm{d}p}{\mathrm{d}z} \quad (0 < r < R), \tag{2.2}$$

where $v_z(r)$ is the axial velocity component and $\dot{\gamma} = \mathrm{d}v_z/\mathrm{d}r$. Solving (2.2) for $\mu(r)$ we obtain the expression for the viscosity distribution given by

$$\mu(r) = \frac{r}{2}\left(\frac{\mathrm{d}v_z}{\mathrm{d}r}\right)^{-1}\frac{\mathrm{d}p}{\mathrm{d}z} \quad (0 < r < R). \tag{2.3}$$

Evaluating (2.3) at $r = R$ and solving for $\mathrm{d}p/\mathrm{d}z$, we find

$$\frac{\mathrm{d}p}{\mathrm{d}z} = \frac{2\mu_R}{R}\left.\frac{\mathrm{d}v_z}{\mathrm{d}r}\right|_{r=R}, \tag{2.4}$$

where $\mu_R = \mu(R)$ is the viscosity at the tube wall. Applying L'Hopital's rule to (2.3) in the limit as $r \to 0$, we obtain an alternative expression for $\mathrm{d}p/\mathrm{d}z$ given by

$$\frac{\mathrm{d}p}{\mathrm{d}z} = 2\mu_0\left.\frac{\mathrm{d}^2v_z}{\mathrm{d}r^2}\right|_{r=0}, \tag{2.5}$$

where $\mu_0 = \mu(0)$ is the centreline viscosity. Combining (2.4) and (2.5) provides an expression for the normalized centreline viscosity given by

$$\frac{\mu_0}{\mu_R} = \frac{(\mathrm{d}v_z/\mathrm{d}r)|_{r=R}}{R(\mathrm{d}^2v_z/\mathrm{d}r^2)|_{r=0}}. \tag{2.6}$$

Combining (2.3) and (2.4) we find that $\mu(r)$ can be expressed independently of $\mathrm{d}p/\mathrm{d}z$ and takes the form

$$\frac{\mu(r)}{\mu_R} = \frac{r}{R}\frac{(\mathrm{d}v_z/\mathrm{d}r)|_{r=R}}{\mathrm{d}v_z/\mathrm{d}r} = \frac{r}{R}\frac{\dot{\gamma}(R)}{\dot{\gamma}(r)} \quad (0 < r < R). \tag{2.7}$$

For the special case of Poiseuille flow, $\dot{\gamma} = \mathrm{d}v_z/\mathrm{d}r$ is linearly proportional to r and the right-hand side of (2.7) reduces to unity. The general result (2.7) applies equally well to distributions in $\mathrm{d}v_z/\mathrm{d}r$ that are nonlinear functions of r, providing that the flow is axisymmetric. This result provides the basis for our local viscosity estimate over the tube cross-section. From μ-PIV measurements in a steady flow of blood through glass capillary tubes, the velocity distribution can be obtained and, from it, so can the viscosity distribution using (2.7).

The relative variation in $\mu(r)$ over the tube cross-section is determined by (2.6); however, the absolute value of $\mu(r)$ depends on μ_R. In the case of a particulate suspension, μ_R corresponds to the dynamic viscosity of the suspension medium, provided that the viscosity of that medium is constant. For a homogeneous fluid having a spatially varying viscosity, μ_R could be regarded as a calibration constant that is chosen in such a way as to minimize the difference between the measured and predicted values of $\mathrm{d}p/\mathrm{d}z$. In the case of blood, the suspension medium consists of plasma, which itself is a suspension containing plasma proteins and glycans. Although plasma viscosity measured with rotational viscometers appears to be independent of shear rate (Chien *et al.* 1966), the method developed here appears to be sensitive enough to reveal a slightly non-uniform viscosity over the cross-section of glass tubes 30–50 μm in diameter perfused with pure plasma under physiologically relevant flow conditions (Long *et al.* 2004). Calibrating μ_R to minimize the least-squares error between measured and predicted values of $\mathrm{d}p/\mathrm{d}z$ has shown that, in the case of human blood, μ_R is approximately 95% of the plasma viscosity that would be obtained from a capillary viscometer (Long *et al.* 2004), which is typically found to be $\sim 0.01\,\mathrm{dyn\,s\,cm^{-2}}$ for human plasma at 25 °C.

2.3. *The velocity distribution*

Although the velocity profile is to be extracted from velocimetry data, it is nevertheless useful to derive an expression for $v_z(r)$, as this will be useful later in fitting the μ-PIV data. The boundary-value problem for $v_z(r)$ is obtained in the usual way by substituting the constitutive relationship for τ_{rz} into the momentum equation given by (2.1) and applying suitable boundary conditions. Thus, we obtain

$$\frac{1}{r}\frac{\mathrm{d}}{\mathrm{d}r}(r\tau_{rz}) = \frac{1}{r}\frac{\mathrm{d}}{\mathrm{d}r}\left(\mu(r)\,r\frac{\mathrm{d}v_z}{\mathrm{d}r}\right) = \frac{\mathrm{d}p}{\mathrm{d}z} \quad (0 < r < R), \tag{2.8}$$

with the no-slip boundary and axisymmetry conditions given, respectively, by

$$v_z(r = R) = 0, \qquad \left.\frac{\mathrm{d}v_z}{\mathrm{d}r}\right|_{r=0} = 0. \tag{2.9}$$

For unidirectional flow in the axial direction, the radial momentum equation requires that the pressure, p, is at most a function of z only. In light of this, it is evident from (2.8) that the axial component of the pressure gradient, $\mathrm{d}p/\mathrm{d}z$, must be constant and therefore p must be a linear function of z. The solution, v_z, that satisfies (2.8) subject to (2.9) for arbitrary $\mu(r)$ is given by

$$v_z(r) = v_{max}\int_r^R \frac{\sigma\,\mathrm{d}\sigma}{\mu(\sigma)/\mu_R}\left(\int_0^R \frac{\sigma\,\mathrm{d}\sigma}{\mu(\sigma)/\mu_R}\right)^{-1} \quad (0 < r < R), \tag{2.10}$$

where v_{max} is the magnitude of the axial velocity component along the tube centreline at $r = 0$, and σ is a dummy variable of integration.

2.4. *The relative apparent viscosity*

Integrating (2.10) over the tube cross-section and applying mass conservation, we obtain the constant volume-flow rate, Q, given by

$$Q = 8Q_P \int_0^1 \int_{r^*}^1 \frac{\sigma^* \, \mathrm{d}\sigma^*}{\mu(\sigma^*)/\mu_R} r^* \, \mathrm{d}r^*, \tag{2.11}$$

where $r^* = r/R$, $\sigma^* = \sigma/R$, and $Q_P = -\pi R^4(\mathrm{d}p/\mathrm{d}z)/(8\mu_R)$ is the volume-flow rate for Poiseuille flow of a fluid having constant viscosity, μ_R. We define the relative apparent viscosity, η_{rel} as the ratio Q_P/Q. Using (2.11), we obtain

$$\eta_{rel} = \frac{\mu_{app}}{\mu_R} := \frac{Q_P}{Q} = \left(8 \int_0^1 \int_{r^*}^1 \frac{\sigma^* \, \mathrm{d}\sigma^*}{\mu(\sigma^*)/\mu_R} r^* \, \mathrm{d}r^* \right)^{-1}, \tag{2.12}$$

where, upon replacing r by $\sigma^* R$, the normalized viscosity distribution, $\mu(\sigma^*)/\mu_R$, is given by the right-hand side of (2.7). In (2.12), μ_{app} is the apparent viscosity defined as the viscosity required to satisfy Poiseuille's law relating pressure drop to volume flow in a tube of radius R.

2.5. *The tube and discharge haematocrits*

The mean instantaneous red-cell fraction per unit tube length and the mean red-cell flux fraction per unit tube length correspond, respectively, to the tube haematocrit, H_T, and discharge haematocrit, H_D, defined by

$$H_T = \frac{1}{A} \int\int_A H \, \mathrm{d}A, \quad H_D = \frac{1}{Q} \int\int_A H v_z \, \mathrm{d}A, \tag{2.13}$$

where Q is given by (2.11), A denotes the tube cross-sectional area, and H is the local haematocrit at a point in the cross-section. For axisymmetric velocity and haematocrit distributions, the ratio of tube-to-discharge haematocrits is then given by

$$\frac{H_T}{H_D} = \frac{Q}{A} \frac{\displaystyle\int_0^R H(r) r \, \mathrm{d}r}{\displaystyle\int_0^R H(r) v_z(r) r \, \mathrm{d}r}. \tag{2.14}$$

From our predicted viscosity distribution, $\mu(r)$, it is possible to infer the haematocrit distribution, $H(r)$, using relationships obtained from *in vitro* species-specific viscometric data of red blood cell suspensions in plasma (Chien *et al.* 1966). As mentioned earlier, for shear-rate distributions typical of the microcirculation (Long *et al.* 2004), shear rates often exceed $50\,\mathrm{s}^{-1}$ over $\sim 90\%$ of the vessel cross-section. Under such conditions, it might be reasonable to neglect variations in blood viscosity with shear rate at a fixed haematocrit, but nevertheless account for its nonlinear variation with haematocrit (Chien *et al.* 1966). Thus, we regard $H(\mu)$ as being readily obtainable from a shear-rate-independent transport relation that can be used in combination with (2.7) and (2.11) to determine H_T and H_D as defined by (2.13).

Since $\mathrm{d}p/\mathrm{d}z$, H_T, H_D and η_{rel} are extremely difficult, if not impossible, to accurately measure *in vivo* (Lipowsky *et al.* 1978, 1980; Desjardins & Duling 1987), the present approach provides a means of estimating these quantities from measured *in vivo* microvascular velocity distributions (Tangelder *et al.* 1988; Long *et al.* 2004). Furthermore, since these quantities can be directly measured *in vitro*, this approach offers the opportunity to interrogate the validity of the model, and the continuum fluid

approximation in particular, through comparison of theoretical predictions with a variety of quantities that are directly measurable *in vitro* (Long *et al.* 2004). We have therefore established a model that can be thoroughly tested *in vitro* on the one hand, and has tremendous predictive potential *in vivo* on the other.

In order to extend the analysis presented here to blood flow in microvessels *in vivo*, a generalization is required to account for the haemodynamic influence of the glycocalyx surface layer on the luminal vessel wall (Vink & Duling 1996; Pries *et al.* 1997; 2000; Smith *et al.* 2003). While the analysis presented in this section applies throughout the lumen of glass capillary tubes, in microvessels it is limited to the cross-sectional region extending up to, but not including, the region near the vessel wall occupied by the glycocalyx. In the following section, we generalize and couple the preceding analysis to an analysis of plasma flow through the glycocalyx.

3. Microhaemofluidics in microvessels

With only slight modifications, many of the equations derived in § 2 can be adapted to the problem of a cylindrical tube lined with a uniformly thick porous layer. The glycocalyx-lined microvessel will be modelled as a straight cylindrical tube of radius R lined, on its luminal surface, with a porous layer having uniform permeability, k, and uniform thickness, $R-a$, where a is the radial location of the blood/glycocalyx 'interface'. We regard the thickness and permeability as being representative of the mean values associated with a glycocalyx that varies axially in thickness and axially and radially in permeability. Hereinafter, $R-a$ and k will denote the effective hydrodynamically relevant thickness and effective permeability, respectively. This idealization is nevertheless quantitatively useful since it follows, from the mean-value theorem for integrals of continuous functions, that these parameters are bounded by the largest and smallest values they would assume in a heterogeneous, spatially non-uniform glycocalyx.

Invoking this model geometry, we identify two distinct regions, which we refer to as the free lumen, where $0 \leqslant r \leqslant a$, and the annular porous layer, where $a \leqslant r \leqslant R$. Within the free lumen, as with the *in vitro* case, we again assume a fully developed axisymmetric steady tube flow of a linearly viscous incompressible isotropic fluid with radially varying viscosity, $\mu(r)$, where the momentum equation for the axial velocity component, $v_z^l(r)$, is given by (2.8) after replacing v_z with v_z^l and R with a. We assume that red cells cannot penetrate the glycocalyx (Vink & Duling 1996) and model flow in the porous layer with the Brinkman equation (Damiano *et al.* 1996; 2004; Feng & Weinbaum 2000). Under these flow conditions, the axial fluid velocity component, $v_z^f(r)$, in the porous layer is governed by

$$\frac{\mu_a}{r}\frac{\mathrm{d}}{\mathrm{d}r}\left(r\frac{\mathrm{d}v_z^f}{\mathrm{d}r}\right) - K\,v_z^f = \frac{\mathrm{d}p}{\mathrm{d}z} \quad (a < r < R), \tag{3.1}$$

where $\mu_a = \mu(a)$ is the viscosity at the interface between the glycocalyx and plasma in the free lumen and K is the hydraulic resistivity of the Brinkman medium, which is inversely proportional to the permeability, k.

Invoking the Brinkman equation (rather than a more general description using something like mixture theory) as a first approximation to model the glycocalyx is likely to be reasonable when we consider the very low solid-volume fractions the layer is thought to have *in vivo* (Damiano *et al.* 1996; Feng & Weinbaum 2000). It is not uncommon for mucopolysaccharide structures devoid of collagen to contain solid-volume fractions less than 1%. In such a case, the viscosity of the fluid constituent

within these structures is very nearly equal to that of the external fluid. We therefore assume that the viscosity of the fluid in the Brinkman-medium model is simply equal to μ_a. Even with very low solid-volume fractions, the permeability of the porous layer can nevertheless be sufficiently low (Damiano *et al.* 1996) that the Darcy term dominates the left-hand side of (3.1) throughout most of the layer, except very near solid boundaries and fluid interfaces.

Assuming, as we have, that red cells cannot penetrate the glycocalyx, then $H(r)=0$ and $\mu=\mu_a$ on $a\leqslant r\leqslant R$. In the free lumen, (2.3)–(2.7) apply if v_z is replaced by v_z^l and R is replaced by a. The solutions for v_z^l and v_z^f were given by Damiano *et al.* (1996) for a constant-viscosity fluid in the free lumen and later generalized to a spatially varying fluid viscosity in the free lumen by Damiano (1998). In the limit as the fluid volume fraction in the porous layer approaches unity, the velocity distributions are given by

$$v_z^l(r^*) = v_{slip}\left(1-\frac{1}{2G(\alpha)}\int_{r^*}^{\alpha}\frac{\sigma^*\,\mathrm{d}\sigma^*}{\mu(\sigma^*)/\mu_a}\right)\quad(0\leqslant r^*\leqslant\alpha),\tag{3.2}$$

and

$$v_z^f(r^*) = v_{slip}\frac{G(r^*)}{G(\alpha)}\quad(\alpha\leqslant r^*\leqslant 1),\tag{3.3}$$

where $\alpha=a/R$, $v_{slip}=v_z^l(\alpha)=v_z^f(\alpha)$ is the slip velocity at the effective hydrodynamic interface between the free lumen and glycocalyx,

$$G(r^*)=\frac{1}{\kappa^2}\left\{\left(\tfrac{1}{2}\kappa\,\alpha+\frac{K_1(\kappa\alpha)}{K_0(\kappa)}\right)\frac{I_0(\kappa r^*)-\beta K_0(\kappa r^*)}{I_1(\kappa\alpha)+\beta K_1(\kappa\alpha)}+\frac{K_0(\kappa r^*)}{K_0(\kappa)}-1\right\}\quad(\alpha\leqslant r^*\leqslant 1),$$

$\beta=I_0(\kappa)/K_0(\kappa)$, and the dimensionless hydraulic resistivity, $\kappa^2=KR^2/\mu_a$. Here, I_n and K_n are the modified, integer-order Bessel functions of the first and second kind, respectively.

As with flow in glass tubes, we can obtain expressions for $\mathrm{d}p/\mathrm{d}z$, η_{rel} and H_T/H_D that depend only on μ-PIV data obtained within the free lumen *in vivo*. The slip velocity, v_{slip}, can also be estimated from μ-PIV data, as described in §4. The total volume flow, Q, through the microvessel is the sum of the volume flow, Q^l, in the free lumen and the volume flow, Q^f, in the porous layer where Q^l and Q^f are determined from (3.2) and (3.3) to be

$$Q^l=\pi R^2 v_{slip}\int_0^{\alpha}\left(2-\frac{1}{G(\alpha)}\int_{r^*}^{\alpha}\frac{\sigma^*\,\mathrm{d}\sigma^*}{\mu(\sigma^*)/\mu_a}\right)r^*\,\mathrm{d}r^*\tag{3.4}$$

and

$$Q^f=\pi R^2(1-\alpha^2)v_{slip}\bar{v}^{*f}\tag{3.5}$$

where $\bar{v}^{*f}$, defined as the dimensionless mean velocity of plasma flow through the porous layer per unit slip velocity, depends only on α and κ and is given by

$$\bar{v}^{*f}=\frac{1}{C_1}\left(\frac{1}{2}+\frac{\kappa(K_1(\kappa)-\alpha K_1(\alpha\kappa))}{K_0(\kappa)(1-\alpha^2)}+\frac{\kappa\,C_2}{1-\alpha^2}\left(\alpha-\frac{I_1(\kappa)+\beta K_1(\kappa)}{I_1(\alpha\kappa)+\beta K_1(\alpha\kappa)}\right)\right),\tag{3.6}$$

where

$$C_1=1-\frac{K_0(\alpha\kappa)}{K_0(\kappa)}-C_2\frac{I_0(\alpha\kappa)-\beta K_0(\alpha\kappa)}{I_1(\alpha\kappa)+\beta K_1(\alpha\kappa)},\quad C_2=\frac{\alpha}{2\kappa}\frac{\mu_0}{\mu_a}+\frac{K_1(\alpha\kappa)}{K_0(\kappa)}.$$

Replacing v_z by v_z^l and R by a in the expression for $\mathrm{d}p/\mathrm{d}z$, given by (2.4), and using this in Q_P, we obtain

$$Q_P = -\frac{\pi R^2}{4\alpha}\frac{\mathrm{d}v_z^l}{\mathrm{d}r^*}\bigg|_{r^*=\alpha}.$$

Using this in the definition for η_{rel} given in (2.12) we obtain

$$\begin{aligned}\eta_{rel} &= -\frac{\pi R^2}{4\alpha Q}\frac{\mathrm{d}v_z^l}{\mathrm{d}r^*}\bigg|_{r^*=\alpha} \\ &= -\frac{1}{8\,G(\alpha)}\left(\int_0^\alpha\left(2-\frac{1}{G(\alpha)}\int_{r^*}^\alpha\frac{\sigma^*\,\mathrm{d}\sigma^*}{\mu(\sigma^*)/\mu_a}\right)r^*\,\mathrm{d}r^* + (1-\alpha^2)\bar{v}^{*f}\right)^{-1}, \quad (3.7)\end{aligned}$$

where we have used the sum of (3.4) and (3.5) to determine Q. Finally, the expressions for H_T, H_D, and the ratio H_T/H_D, given by (2.13) and (2.14), apply in microvessels if v_z is replaced by v_z^l, R is replaced by a, and Q is replaced by the sum of (3.4) and (3.5).

As with the relations in § 2, these relationships satisfy the conservation principles of mass and momentum in the free lumen and porous layer. Two parameters that do not appear in the glass tube model are the dimensionless layer thickness, $1-\alpha = 1-a/R$, and the dimensionless hydraulic resistivity of the glycocalyx, $\kappa^2 = KR^2/\mu_a$. While estimates of both of these quantities are available for skeletal-muscle capillaries (Vink & Duling 1996; Feng & Weinbaum 2000; Damiano & Stace 2002) and more recently for post-capillary venules (Smith *et al.* 2003), the analysis presented here provides an objective method for obtaining independent estimates of these quantities from *in vivo* μ-PIV data as described below (Long *et al.* 2004).

The viscosity, μ_a, in the analysis of glycocalyx-lined microvessels is directly analogous to μ_R in the smooth-walled-tube analysis of § 2. As such, it is taken to be equal to the plasma viscosity as measured by a standard capillary viscometer. However, the very presence of the glycocalyx itself in microvessels could significantly alter plasma rheology *in vivo* in such a way as to call into question this similarity to glass tube studies. In light of the great variety of known binding sites on the glycocalyx to the numerous plasma macromolecules in blood, a polymerization of blood plasma might be possible in glycocalyx-lined microvessels that would not occur in smooth-walled glass tubes. However unlikely it may seem, such a polymerization cannot and should not be ruled out unless definitive evidence to the contrary can be established. Methods developed here could be employed to test this hypothesis if μ-PIV data were collected in microvessels from which red cells, but not particle tracers, had been diverted. If velocity and viscosity distributions obtained in the free lumen of such vessels were consistent with those found in capillary glass tube studies (Long *et al.* 2004), it would suggest that any polymerization of plasma that might arise *in vivo* is of little consequence to the microhaemofluidics described here.

While the preceding analysis has been limited to steady flow conditions, this assumption can be relaxed such that the analytical results developed here can be applied directly, without modification, to many periodic unsteady microscale flow regimes. Whereas flow in venules is very nearly steady, by triggering data acquisition of the particle tracers in the flow with the corresponding peak flow in the cardiac cycle, this analysis can be applied directly to pulsatile flows in arterioles, since, under normal physiological conditions, unsteady inertial forces are negligibly small compared with viscous forces in arterioles less than 200 μm in diameter (El-Khatib & Damiano 2003). Implicit in this section, therefore, is the understanding that, with careful attention to

data acquisition, the analytical results presented here apply generally to blood flow in microvessels, including both venules and arterioles, greater than $\sim 20\,\mu$m in diameter.

4. Implementation using μ-PIV data

For the laminar, steady, fully developed flow regimes considered here, data sufficient to extract accurate velocity distributions can be obtained from measurements of the radial position and axial speed of ~ 50–100 microspheres randomly distributed over the vessel cross-section. For flow rates typical of skeletal-muscle venules *in vivo*, these data can be collected from digital or video recordings in < 30 s (Long *et al.* 2004).

4.1. *Data analysis*

Most microspheres in a given data set lie somewhat out of the midsagittal plane of the vessel. If such a microsphere has a true radial position, r, its image, when projected into the midsagittal plane, will have a corresponding measured radial distance, ρ, from the vessel centreline. In general, $r \geqslant \rho$, where equality holds only for microspheres lying in the midsagittal plane. For a given data set, an optimal subset of the data can be found that best reflects the true local fluid velocities in the midsagittal plane by recognizing that these velocity distributions decrease monotonically with increasing r so that microspheres nearest to the midsagittal plane travel faster than any others having the same measured value of ρ or any other measured value of ρ that is further from the vessel centreline. Therefore, data points that are to be retained must satisfy this criterion. Accordingly, all of the data are filtered such that the reduced data set consists of all of the N possible measurements that satisfy

$$v_i^m(\rho_i) > v_{i+1}^m(\rho_{i+1}) \quad \text{for} \quad \rho_i < \rho_{i+1} \quad (i = 1, 2, \ldots, N-1), \tag{4.1}$$

where $v_i^m(\rho_i)$ is the measured axial speed of the ith microsphere at the measured radial distance, ρ_i, from the vessel centreline. Typically, ~ 20–30% of the microspheres in a data set will satisfy this criterion (Long *et al.* 2004).

4.2. *Regression analysis*

A fit to these N data points, using a standard nonlinear regression analysis, provides the best possible approximation to the cross-sectional velocity profile in the midsagittal plane that can be extracted from the data. Rotation of this profile about the z-axis provides the surface of revolution that best reflects the three-dimensional axisymmetric velocity profile over the vessel cross-section. The fit itself, however, must satisfy certain constraints in order to be consistent with various assumptions and conditions laid out in the analysis. In particular, it must be continuous and axisymmetric. Furthermore, fits to data from cylindrical tubes must satisfy the no-slip condition, such that $v_z = 0$ at $r = R$, whereas fits to data from microvessels must satisfy the pseudoslip condition at the glycocalyx interface, such that $v_z^l = v_{slip}$ at $r = a$. Furthermore, fits to data from microvessels must also satisfy the condition that the shear stress be continuous across the glycocalyx interface (Damiano *et al.* 1996). Functions that satisfy all of these conditions have already been found and are given by (2.10) and (3.2) to within the arbitrary function, $\mu(r)$. They have the added advantage of satisfying the axial momentum equations. To simplify implementation, we represent the integrands in (2.10) and (3.2) with a fitting function, $f(r^*) = r^* \mu_a / \mu(r^*)$, which necessarily vanishes at $r^* = 0$ and is α at $r^* = \alpha$ (where $\alpha = 1$ for glass tubes). A suitable form for f must satisfy these two conditions and should include both a linear and exponential dependence on r^*. When integrated, such a function would yield a velocity distribution

that contains the necessary quadratic behaviour near the origin to satisfy the symmetry condition and the nonlinear behaviour necessary to fit the data in regions where the shear rate varies nonlinearly with radial position. Thus we propose fitting the data with a function of the form

$$v_{fit}(r^*) = v_{max}\left(2G(\alpha) - \int_{r^*}^{\alpha} f(\sigma^*)\,\mathrm{d}\sigma^*\right)\left(2G(\alpha) - \int_{0}^{\alpha} f(\sigma^*)\,\mathrm{d}\sigma^*\right)^{-1} \quad (0 \leqslant r^* \leqslant \alpha), \tag{4.2}$$

using the fitting function $f(r^*) = r^*(1 - c_1 \sinh c_2\,\alpha) + \alpha c_1 \sinh c_2 r^*$, where c_1 and c_2 are found through nonlinear regression analysis that uses (4.2) to minimize the least-squares error in the fit to the N data points identified above. The parameter v_{max}, corresponding to the axial centreline velocity, is found by replacing (r^*, v_{fit}) in (4.2) with $(\rho_i/R, v_i^m)$ from the reduced μ-PIV data set, solving for v_{max} for each $i = 1, 2, \ldots, N-1$, and taking the average of all computed v_{max} values. It should be noted that the first term on the right-hand side of (4.2) represents the slip velocity at $r = \alpha$. For flow in a glass tube, $\alpha = 1$, and since $G(1) = 0$, the slip velocity in (4.2) vanishes and (4.2) satisfies the no-slip condition at the tube wall. The function v_{fit} and its derivatives are continuous on $0 \leqslant r^* \leqslant \alpha$.

4.3. *Implementation in glass tubes*

Performing the regression analysis described above on μ-PIV data obtained from blood flow in glass tubes, the parameters c_1 and c_2 can be determined and v_{fit}, given by (4.2), can then be substituted for v_z in (2.7) to extract the viscosity profile given by

$$\frac{\mu(r)}{\mu_R} = \frac{r}{R}\frac{(\mathrm{d}v_{fit}/\mathrm{d}r)|_{r=R}}{\mathrm{d}v_{fit}/\mathrm{d}r} \quad (0 \leqslant r \leqslant R). \tag{4.3}$$

This result can then be used in (2.12) to determine η_{rel}. It can also be used to determine $H(r^*)$, provided there exists a correlation function of the form $H(\mu(r^*))$ that can be derived from a transport relation obtained from high-shear-rate rotational viscometric data for red blood cell suspensions in plasma (Chien *et al.* 1966). With the distribution $H(r^*)$ determined, substitution of (4.2) for v_z in (2.13) provides estimates of H_T and H_D. Furthermore, v_{fit} can be substituted for v_z in (2.4) to estimate $\mathrm{d}p/\mathrm{d}z$.

4.4. *Implementation in microvessels*

The regression analysis used to determine the parameters c_1 and c_2 based on μ-PIV data obtained from blood flow in microvessels parallels the methods described above in glass tubes with the notable exception that the fit obtained for a given data set must, in some sense, correspond to the best possible fit in the two-dimensional parameter space (α, κ). One approach might be to choose a particular value of κ and then iteratively search for the corresponding value of α that results in v_{fit}, given by (4.2), minimizing the least-squares error in the fit to a particular data set for all possible choices of α. Once the value α_{min} corresponding to this minimum is found for a given κ, the quantities $G(r)$ and $\bar{v}^{*f}$ are both determined, as is the velocity distribution, $v_z^f(r)$, throughout the layer. The average value of $1 - \alpha_{min}$ across many vessels would provide an estimate of the dimensionless mean thickness of the layer for a given κ. A similar minimization involving the parameter κ could also be performed. For a given pair (α_{min}, κ), the corresponding parameters c_1 and c_2 are determined as is v_{fit} given by (4.2). The viscosity distribution is then obtained from (4.3) after substituting a for

R. With v_{fit} and $\mu(r)$ determined, all other properties of the flow follow from (2.13) and (3.4)–(3.7).

4.5. *Near-wall microfluidics*

When μ-PIV is used to extract the velocity distribution, careful consideration must be given to the role of near-wall microfluidics on the motion of microspheres closest to the tube or vessel wall. Throughout most of the flow field, the tube or vessel wall exerts very little influence on the motion of microspheres relative to the fluid, and thus most of the microspheres essentially reflect the local fluid–particle velocity that would arise in the absence of particle tracers in the flow. However, the enhanced drag exerted on near-wall microspheres due to the presence of the tube or vessel wall should be accounted for in the analysis. In particular, since the microspheres themselves influence near-wall microfluidics, the problem becomes how to use particle-tracer data to extract the true fluid velocity distribution that would arise in the absence of microspheres.

Detailed three-dimensional analyses have been carried out on the translational and rotational motions of a sphere in a Stokes flow travelling near a smooth planar confining boundary (Dean & O'Neill 1963; O'Neill 1964) and near a Brinkman half-space (Damiano *et al.* 2004). Results of these analyses were used to study the particular case of the free motion of a neutrally buoyant sphere in a uniform shear field travelling parallel to a smooth planar confining boundary (Goldman, Cox & Brenner 1967) and a Brinkman half-space (Damiano *et al.* 2004). In the case of the former, the disparity between the translational speed of a sphere, with its centre located at a distance of one or more sphere diameters away from a smooth planar confining boundary, and a fluid particle located at this distance from the plane if the sphere were not present in the flow, is less than 5% (Goldman *et al.* 1967). This disparity is even smaller when the sphere centre is one or more sphere diameters from a Brinkman half-space (Damiano *et al.* 2004). In the context of microvascular haemodynamics, it is implied that all reference to μ-PIV data in foregoing and subsequent discussions is made with the understanding that these data have been transformed to fluid–particle velocities using either the results of Goldman *et al.* (1967), for blood flow in glass capillary tubes, or the results of Damiano *et al.* (2004), for blood flow in glycocalyx-lined microvessels. Detailed methods for systematically transforming μ-PIV data into local fluid–particle velocities are given by Smith *et al.* (2003).

5. Application to microvascular haemodynamics

The development of the analytical tools presented here was motivated by their particular application to the study of microhaemofluidics in microvessels. By way of illustrating their usefulness in this context, we present in this section an example of how these tools can be used to extract relevant quantitative information on the haemodynamics in microvessels that has otherwise been inaccessible *in vivo*.

5.1. *Data acquisition in microvessels using intravital μ-PIV*

The μ-PIV technique (Santiago *et al.* 1998; Smith *et al.* 2003) that we employ uses stroboscopic double-flash epi-illumination to visualize systemically injected, fluorescently labelled, neutrally buoyant polystyrene microspheres ($\sim 0.5\,\mu$m diameter) circulating in microvessels *in vivo*. Transillumination is maintained to keep the vessel wall visible so that the radial position of each microsphere can be measured relative to the vessel wall. The radial distribution in the velocity of ~ 50–100 microspheres is recorded on videotape over a period of ~ 10–20 s (see figure 1). Detailed methods

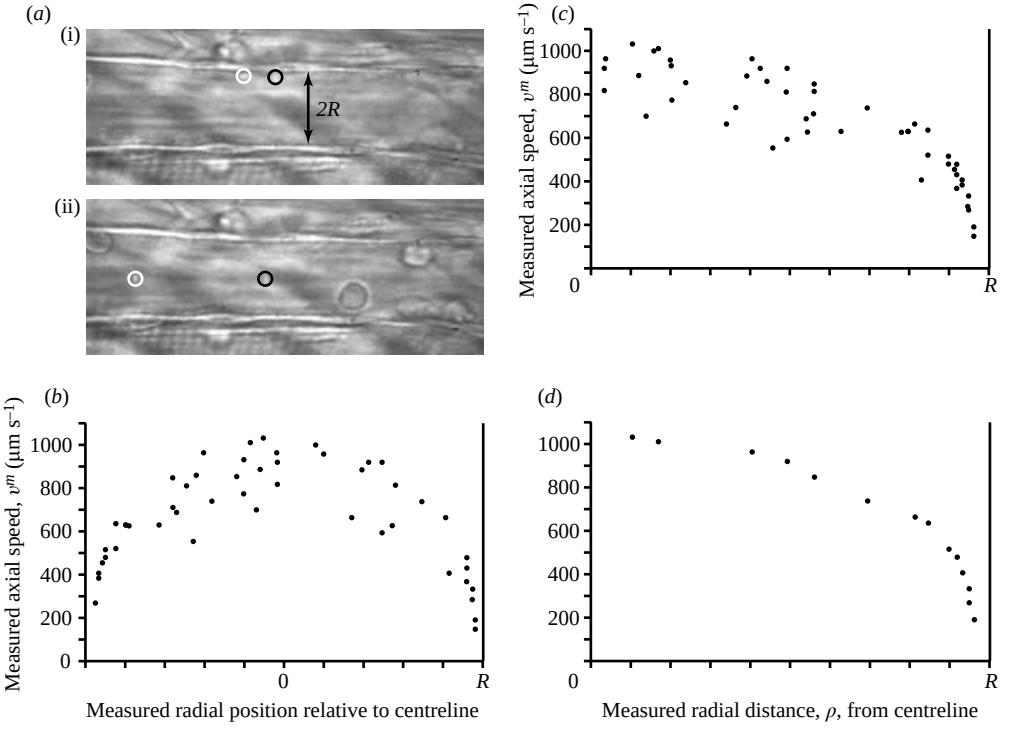

FIGURE 1. (*a*) Typical bright-field images of a microvessel in the mouse cremaster muscle showing dual images of (i) one near-wall microsphere and (ii) one near-centre microsphere. The dual images of each microsphere (encircled in white upstream and black downstream) are separated in time by the double flash interval (5–16.67 ms apart). (*b–d*) Raw μ-PIV data collected over the cross-section of a 21.8 μm-diameter venule in the mouse cremaster muscle after light-dye treatment to degrade the glycocalyx surface layer. (*b*) The complete μ-PIV data set shows the translational speed of each microsphere as a function of its measured radial position relative to the vessel centreline. Since velocity profiles are assumed to be axisymmetric, all μ-PIV data collected over the entire vessel cross-section were folded over to one side of the vessel centreline, as shown in (*c*). Only monotonically filtered data (*d*), obtained using (4.1) on the complete data set in (*c*), were used to extract the velocity profile.

describing the intravital microscopy protocols and the μ-PIV technique are given by Smith *et al.* (2003) and Long *et al.* (2004).

Whereas it is necessary to correct for the optical artefact that arises in the measured radial position of microspheres in glass capillary tubes, this is not the case for μ-PIV data in microvessels *in vivo* (Smith *et al.* 2003; Long *et al.* 2004). Results have shown (Smith *et al.* 2003) that there is no statistically significant difference in the length of radially versus axially aligned erythrocytes in mouse cremaster-muscle venules after flow cessation with a blunt micropipette. On the other hand, a statistically significant difference in the length of radially versus axially aligned erythrocytes has been shown to exist in a quiescent red-cell suspension in glass capillary tubes. This difference was found to be in excellent agreement with the difference predicted using Snell's law (Smith *et al.* 2003). Therefore, while a slight difference in refractive indices certainly does exist between plasma and the surrounding tissue, as evidenced by the fact that the endothelium is visible under brightfield microscopy, this difference produces a negligibly small optical artifact *in vivo*. No optical correction of intravital μ-PIV data

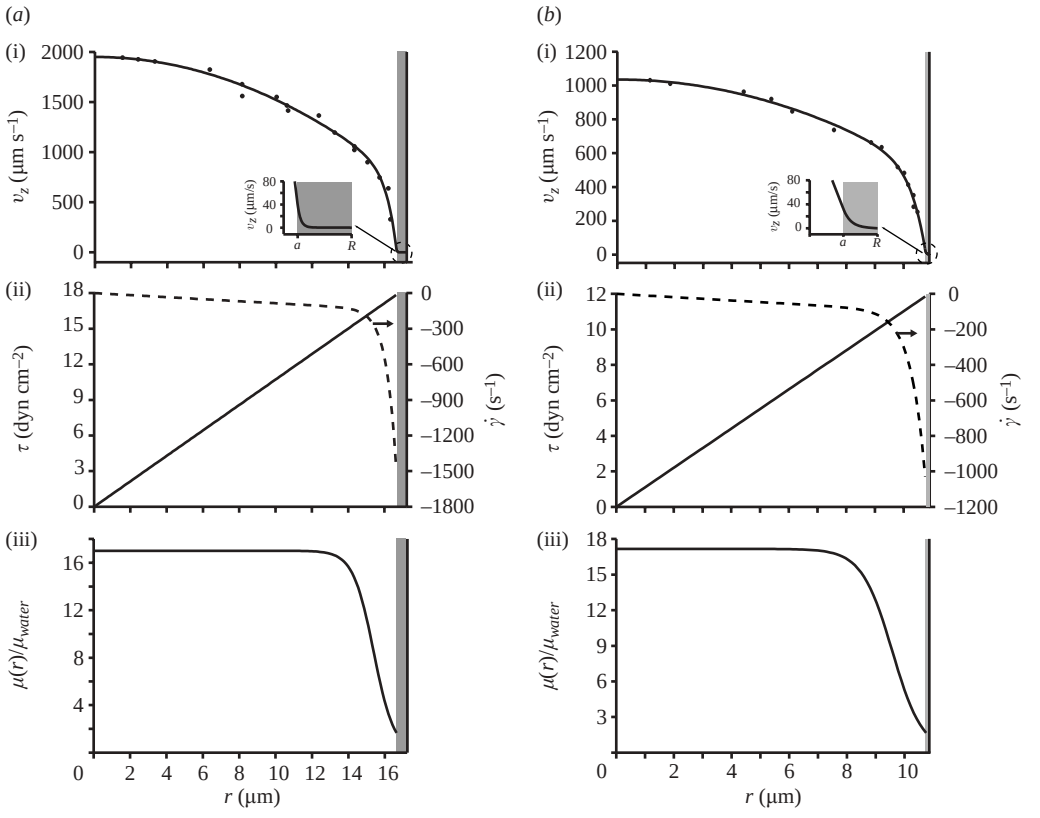

2R (μm)	R – a (μm)	–dp/dz (dyn cm^{-3})	η_{rel}	$\dot{\gamma}(a)/\dot{\gamma}_P(R)$
34.5	0.56	18895	5.15	6.2

2R (μm)	R – a (μm)	–dp/dz (dyn cm^{-3})	η_{rel}	$\dot{\gamma}(a)/\dot{\gamma}_P(R)$
21.8	0.15	21831	4.04	5.4

FIGURE 2. Results from (*a*) a 34.5 μm-diameter control venule and (*b*) a 21.8 μm-diameter venule after light-dye treatment to degrade the ESL in the mouse cremaster muscle. (i) Intravital fluorescent μ-PIV data (symbols) and predicted axisymmetric velocity profiles, v_{fit}, extracted from the μ-PIV data using (4.2). (ii) Predicted distributions in shear-rate, $\dot{\gamma} = \mathrm{d}v_{fit}/\mathrm{d}r$ (dashed, right axes), and shear-stress, τ_{rz} (solid, left axes), which was obtained from (2.2). (iii) Predicted viscosity profiles, $\mu(r)$, obtained from (2.7) and normalized with respect to water viscosity at the animal's body temperature ($\mu_{water} = 0.007$ dyn s cm^{-2} at 37 °C). The shaded region near the vessel wall shows the predicted thickness of the glycocalyx surface layer. Insets in (i) show the predicted velocity distribution through the layer assuming a hydraulic resistivity, K, of 10^9 dyn s cm^{-4}. Tabulated values shown below the distributions for each vessel are calculated based on this value of K. Data shown in (*b*) (i) correspond to those shown in figure 1(*d*). Results in (*a*) are taken from Long *et al.* (2004) and are included here only for the sake of comparison with results of the light-dye treated vessel shown in (*b*).

is therefore necessary and velocity profiles can be extracted directly from a raw data set, such as that shown in figure 1.

5.2. *Analytical results in microvessels in vivo*

Typical examples of the haemodynamically and physiologically relevant information that can be obtained from microvessels *in vivo* using this approach are shown in figure 2 before and after light-dye treatment to degrade the glycocalyx surface

layer. (Detailed methods describing the light-dye treatment technique to degrade the glycocalyx are given by Vink & Duling (1996) and Smith *et al.* (2003).) In particular, using the velocity profile extracted from the monotonically filtered μ-PIV data, we have obtained distributions, similar to those shown in figure 2, in shear rate, shear stress and viscosity over the cross-section of nine light-dye treated venules (19–31 μm i.d.) in the cremaster muscle of three wild type (WT) mice. From these distributions, we used the analytical results described above to estimate, in each of the light-dye treated vessels, the axial pressure gradient component, $\mathrm{d}p/\mathrm{d}z$ (ranging in absolute value from 8807 to 37985 dyn cm^{-3} with a mean absolute value of 23864 ± 2838 dyn cm^{-3} for $K = 10^9$ dyn s cm^{-4}), and the relative apparent viscosity, η_{rel} (ranging from 2.66 to 4.21 with a mean value of 3.43 ± 0.17 for $K = 10^9$ dyn s cm^{-4}). Since flow through the glycocalyx surface layer is so significantly attenuated for $K \geqslant \sim 10^9$ dyn s cm^{-4} (see figure 2), there was very little difference in these results for the higher values of K we considered.

Validation experiments in glass capillary tubes (50–80 μm i.d.) perfused with human red cell suspensions in blood plasma have established the accuracy of this approach in terms of its ability to predict $\mathrm{d}p/\mathrm{d}z$ and η_{rel} (Long *et al.* 2004). Since comprehensive haematocrit-dependent rotational viscometric data do not yet exist for mouse blood, haematocrit distributions, and therefore H_T and H_D, cannot be reported for the results shown in figure 2. Owing to inter-species differences in the mean corpuscular volume of red blood cells, species-specific rotational viscometric data at high rates of shear are required in order to extract the full range of information possible using these methods. As these rotational viscometric data become available for other species, these methods will find uses in a broad range of applications where tube and discharge haematocrits are required.

Another quantity that is often of interest in studies of the microcirculation is the wall shear rate, $\dot{\gamma}(R)$. It has recently become clear, however, that this quantity is not particularly meaningful in the light of new evidence confirming the presence of a hydrodynamically relevant glycocalyx on the walls of microvessels (Pries *et al.* 1997; Smith *et al.* 2003). This structure effectively eliminates plasma flow near the vessel wall and results in a vanishing small wall shear rate (see figure 2). A more relevant quantity for characterizing the prevailing flow conditions in microvessels, first introduced by Smith *et al.* (2003), is the interfacial shear rate, $\dot{\gamma}(a)$, defined as the shear rate evaluated at the effective hydrodynamic interface between the glycocalyx and the plasma in the free lumen. In each of the light-dye treated vessels considered here, $\dot{\gamma}(a)$ (absolute value in the range 416–1833 s^{-1} with a mean absolute value of 1237 ± 158 s^{-1} for $K = 10^9$ dyn s cm^{-4}) was estimated as was the corresponding wall shear rate, $\dot{\gamma}_P(R)$, that would arise in a Poiseuille flow having a maximum velocity equal to the centreline velocity found in a given vessel. Results showed that, over all of the light-dye treated vessels analysed, $\dot{\gamma}(a)$ was 3.3 to 5.4 times greater than $\dot{\gamma}_P(R)$ (with a mean of 4.2 ± 0.2). The variation in the ratio of $\dot{\gamma}(a)/\dot{\gamma}_P(R)$, which was reported to be even greater in the control vessels analysed by Long *et al.* (2004), is attributable to normal physiological variation in the red cell concentration that individual microvessels receive within a microvascular network.

5.3. *Viscosity distributions*

The predicted viscosity distributions shown in figure 2 reflect the non-uniform distributions in red blood cells that were present in these microvessels. As proposed earlier, these viscosity profiles can be used to infer haematocrit profiles, and thus

H_T and H_D using (2.13), once comprehensive species-specific rotational viscometric data become available. In the absence of such data for mouse blood, we confine our discussion here to qualitative observations about the haematocrit profile and its implications for H_T and H_D. If viscometric data for human blood were used to estimate $H(r)$ in both the control and light-dye treated vessels shown in figure 2, the predicted values of H_T and H_D would be $< \sim 55\%$ and $< \sim 62\%$, respectively. However, based on recently obtained rotational viscometric data of mouse and human red blood cells suspended in autologous blood plasma (Long, Smith, Ley & Damiano, unpublished data), we would expect these values to be somewhat lower if correlation functions for mouse blood were used. Discharge haematocrits of 50–60% are at the high end of the physiological normal range that we might expect in these microvessels (Desjardins & Duling 1987).

5.4. *Estimation of the glycocalyx thickness in vivo*

A remarkable result of this analysis is its ability to predict the hydro-dynamically effective thickness of the glycocalyx surface layer *in vivo*. For each light-dye treated vessel and particular value of K, we determined the layer thickness that corresponded to the minimum least-squares error in the fit to the μ-PIV data as described earlier. We found that glycocalyx thickness estimates in light-dye treated vessels ranged between 0.1 and 0.3 μm with a mean value of 0.2 ± 0.02 μm for $K = 10^9$ dyn s cm^{-4}. Long *et al.* (2004) reported thickness estimates in the control vessels in the range of 0.3–0.7 μm with a mean value of 0.5 ± 0.03 μm for $K = 10^9$ dyn s cm^{-4}. A statistically significant decrease of 0.3 μm in the estimated mean thickness of the glycocalyx was observed after light-dye treatment to degrade the layer. These results are summarized in figure 3 for two finite values of K and for the limiting case of no flow through the layer (i.e. as $K \to \infty$). Estimates of the mean and standard deviation for the control and light-dye treated vessels were insensitive to the value of K over the range of values considered.

Smith *et al.* (2003) considered a subset of the data used here and in Long *et al.* (2004) to investigate the velocity distribution in the plasma-rich region near the vessel wall in both control and light-dye treated microvessels. They considered only those microspheres that were within ~ 2 μm of the vessel wall and assumed that a uniform shear rate existed throughout the plasma-rich region of the vessel up to the glycocalyx interface. Neglecting the effect of red cells and assuming that the fluid viscosity was constant throughout the plasma-rich region and equal to that of blood plasma, their analysis revealed the presence of a strongly exponential rather than linear velocity distribution throughout a region adjacent to the vessel wall, which they proposed was occupied entirely by the glycocalyx surface layer. From these distributions, they were able to provide the first direct estimates of the effective haemodynamically relevant thickness of the layer *in vivo*. Furthermore, they found a statistically significant decrease in their estimate of the layer thickness after light-dye treatment to degrade the glycocalyx.

We regard the results here as being slightly more accurate than those reported by Smith *et al.* (2003), principally because the shear rate distribution in these microvessels is not uniform throughout the plasma-rich region as they had assumed. In fact, in all of the light-dye treated vessels analysed here, and in all of the control vessels reported in Long *et al.* (2004), most of the variation in the shear rate distribution occurs in the plasma-rich region of the vessel (see figure 2). Fitting a linear velocity distribution to the near-wall μ-PIV data, as was done by Smith *et al.* (2003), slightly underestimates the absolute value of the interfacial shear rate. Since the shear rate

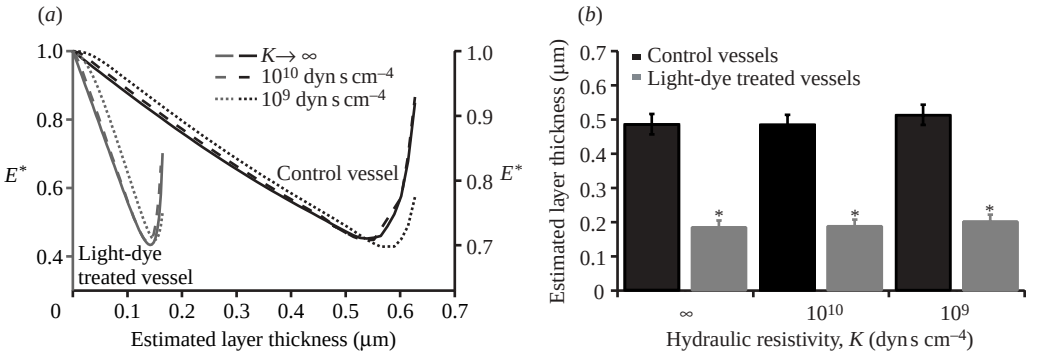

FIGURE 3. (*a*) Variations, relative to the estimated glycocalyx surface-layer thickness, in the normalized least-squares error, E^*, associated with the fits to the μ-PIV data in the 34.5 μm-diameter control venule shown in figure 2(*a*), (black curves) and in the 21.8 μm-diameter light-dye treated venule shown in figure 2(*b*), (grey curves). Each set of three curves shows results for $K = 10^9$ dyn s cm^{-4} (dotted curves), $K = 10^{10}$ dyn s cm^{-4} (dashed curves), and the case of no flow through the layer, $K \to \infty$ (solid curves). Estimated glycocalyx surface-layer thickness for each value of K considered in these two venules corresponds to the value of $R-a$ associated with the local minimum in each of these curves. (*b*) Mean layer thickness of control venules (black; 10 vessels, 24–41 μm diameter, in 4 WT mice) and of light-dye treated venules (grey; 9 vessels, 19–31 μm diameter, in 3 WT mice) obtained from the average of individual estimates of $R - a$, such as those found in (*a*), for two finite values of hydraulic resistivity (10^9 and 10^{10} dyn s cm^{-4}) and for the case of no flow through the layer ($K \to \infty$). *, significant difference via two-tailed t-test ($p < 0.05$).

increases monotonically in absolute value with increasing radial position through the plasma-rich region (up to the glycocalyx interface), the local velocity gradient is a maximum at $r = a$ and will slightly exceed the average gradient corresponding to the slope of a linear regression to all of the μ-PIV data in the plasma-rich region. Extrapolation of the local velocity gradient at $r = a$ would result in a more negative intercept at the vessel wall than the linear regression analysis would predict. This, in turn, would correspond to a slightly thicker and more accurate glycocalyx estimate for each value of K than the estimates Smith *et al.* (2003) were able to provide using a linear regression analysis. One advantage of the near-wall μ-PIV approach presented by Smith *et al.* (2003) is that, if flow through the glycocalyx were neglected, the method is not limited to axisymmetric velocity distributions and can therefore be applied near vessel bifurcations or adherent leukocytes where significant asymmetric flow regimes may arise.

6. Summary

Typically, rheological data are extracted from force measurements, which do not provide the detailed spatial distributions that this approach offers. The idea advanced here, of using a velocity field to extract rheological data, has applications beyond microvascular haemodynamics to a variety of generalized linearly viscous fluids and particle-suspension flows, including polymer melts, emulsions, extrusion and polymeric drag reduction. To those fluids and particulate suspensions for which the Cauchy stress can be expressed as a linear function of the strain rate tensor, and for which a suitable shear-rate-independent transport relation is available, this method can generally be applied.

The authors convey their appreciation to Arne J. Pearlstein and Klaus Ley for their careful reading of the manuscript and for their valuable insights and suggestions. Partial support for this work was contributed by the Whitaker Foundation, RG-98-0524 and TF-02-0024. M. L. S. was supported by National Institutes of Health grant T32 GM 08715-01A1 to Gordon Laurie and Klaus Ley.

REFERENCES

Chen, D. & Kaul, D. K. 1994 Rheological and hemodynamic characteristics of red cells of mouse, rat and human. *Biorheology* **31**, 103–113.

Chien, S., Usami, S., Taylor, H. M., Lundberg, J. L. & Gregersen, M. I. 1966 Effects of hematocrit and plasma proteins on human blood rheology at low shear rates. *J. Appl. Physiol.* **21**, 81–87.

Cokelet, G. R. 1999 Viscometric, *in vitro*, and *in vivo* blood viscosity relationships: how are they related? *Biorheology* **36**, 343–358.

Damiano, E. R. 1998 Blood flow in microvessels lined with a poroelastic wall layer. In *Poromechanics* (ed. J.-F. Thimus, Y. Abousleiman, A. H. -D. Cheng, O. Coussy & E. Detournay), pp. 403–408. Balkema, Rottderdam.

Damiano, E. R., Duling, B. R., Ley, K. & Skalak, T. C. 1996 Axisymmetric pressure-driven flow of rigid pellets through a cylindrical tube lined with a deformable porous wall layer. *J. Fluid Mech.* **314**, 163–189.

Damiano, E. R., Long, D. S., El-Khatib, F. H. & Stace, T. M. 2004 On the motion of a sphere in a Stokes flow parallel to a Brinkman half-space. *J. Fluid Mech.* **500**, 75–101.

Damiano, E. R. & Stace, T. M. 2002 A mechano-electrochemical model of radial deformation of the capillary glycocalyx. *Biophys. J.* **82**, 1153–1175.

Dean, W. R. & O'Neill, M. E. 1963 A slow motion of viscous liquid caused by the rotation of a solid sphere. *Mathematika* **10**, 13–24.

Desjardins, C. & Duling, B. P. 1987 Microvessel hematocrit: measurement and implications for capillary oxygen transport. *Am. J. Physiol.* **252**, H494–H503.

El-Khatib, F. H. & Damiano, E. R. 2003 Linear and nonlinear analyses of pulsatile blood flow in a cylindrical tube. *Biorheology* **40**, 503–522.

Feng, J. & Weinbaum, S. 2000 Lubrication theory in highly compressible porous media: the mechanics of skiing, from red cells to humans. *J. Fluid Mech.* **422**, 281–317.

Goldman, A. J., Cox, R. G. & Brenner, H. 1967 Slow viscous motion of a sphere parallel to a plane wall—II Couette flow. *Chem. Engng Sci.* **22**, 653–660.

Lipowsky, H. H., Kovalcheck, S. & Zweifach, B. W. 1978 The distribution of blood rheological parameters in the microvasculature of cat mesentery. *Circ. Res.* **43**, 738–749.

Lipowsky, H. H., Usami, S. & Chien, S. 1980 In vivo measurements of 'apparent viscosity' and microvessel hematocrit in the mesentery of the cat. *Microvasc. Res.* **19**, 297–319.

Long, D. S., Smith, M. L., Pries, A. R., Ley, K. & Damiano, E. R. 2004 Microviscometry reveals reduced blood viscosity and altered shear rate and shear stress profiles in microvessels after hemodilution. *Proc. Natl Acad. Sci. USA* **101**, 10060–10065.

Nair, P. K., Hellums, J. D. & Olson, J. S. 1989 Prediction of oxygen transport rates in blood flowing in large capillaries. *Microvasc. Res.* **38**, 269–285.

O'Neill, M. E. 1964 A slow motion of viscous liquid caused by a slowly moving solid sphere. *Mathematika* **11**, 67–74.

Pries, A. R., Neuhaus, D. & Gaehtgens, P. 1992 Blood viscosity in tube flow: dependence on diameter. *Am. J. Physiol.* **263**, H1770–H1778.

Pries, A. R., Secomb, T. W. & Gaehtgens, P. 2000 The endothelial surface layer. *Pflügers Arch.* **440**, 653–666.

Pries, A. R., Secomb, T. W., Jacobs, H., Sperandio, M. B., Osterloh, K. & Gaehtgens, P. 1997 Microvascular blood flow resistance: role of endothelial surface layer. *Am. J. Physiol.* **273**, H2272–H2279.

Santiago, J. G., Wereley, S. T., Meinhart, C. D., Beebe, D. J. & Adrian, R. J. 1998 A particle image velocimetry system for microfluidics. *Exps. Fluids* **25**, 316–319.

Secomb, T. W. 1995 Mechanics of blood flow in the microcirculation. In *Biological Fluid Dynamics* (ed. C. P. Ellington & T. J. Pedley), pp. 305–321. Company of Biologists, Cambridge.

Sharan, M. & Popel, A. S. 2001 A two-phase model for flow of blood in narrow tubes with increased effective viscosity near the wall. *Biorheology* **38**, 415–428.

Smith, M. L., Long, D. S., Damiano, E. R. & Ley, K. 2003 Near-wall μPIV reveals a hydrodynamically relevant endothelial surface layer in venules *in vivo*. *Biophys. J.* **85**, 637–645.

Tangelder, G. J., Slaaf, D. W., Arts, T. & Reneman, R. S. 1988 Wall shear rate in arterioles *in vivo*: least estimates from platelet velocity profiles. *Am. J. Physiol.* **254**, H1059–H1064.

Thomas, H. W. 1962 The wall effect in capillary instruments: an improved analysis suitable for application to blood and other particulate suspensions. *Biorheology* **1**, 41–56.

Vink, H. & Duling, B. R. 1996 Identification of distinct luminal domains for macromolecules, erythrocytes, and leukocytes within mammalian capillaries. *Circ. Res.* **79**, 581–589.